Perspective: Is there a hysteresis during reactive High Power Impulse Magnetron Sputtering (R-HiPIMS)?

K. Strijckmans, F. Moens, and D. Depla

Articles you may be interested in

Perspective: Is there a hysteresis during reactive High Power Impulse Magnetron Sputtering (R-HiPIMS)?

K. Strijckmans, F. Moens, and D. Depla
Department of Solid State Sciences, Ghent University, Krijgslaan 281(S1), 9000 Gent, Belgium

This paper discusses a few mechanisms that can assist to answer the title question. The initial approach is to use an established model for DC magnetron sputter deposition, i.e., RSD2013. Based on this model, the impact on the hysteresis behaviour of some typical HiPIMS conditions is investigated. From this first study, it becomes clear that the probability to observe hysteresis is much lower as compared to DC magnetron sputtering. The high current pulses cannot explain the hysteresis reduction. Total pressure and material choice make the abrupt changes less pronounced, but the implantation of ionized metal atoms that return to the target seems to be the major cause. To further substantiate these results, the analytical reactive sputtering model is coupled with a published global plasma model. The effect of metal ion implantation is confirmed. Another suggested mechanism, i.e., gas rarefaction, can be ruled out to explain the hysteresis reduction. But perhaps the major conclusion is that at present, there are too little experimental data available to make fully sound conclusions. *Published by AIP Publishing.* [http://dx.doi.org/10.1063/1.4976717]

I. INTRODUCTION

A researcher interested in answering the title question will seek for information on this topic. Two pathways are quite popular. The first is to perform experiments, and the second is to set-up a model to describe the process. In both cases, one will look for information in the literature to initiate the work. In this perspective, modelling is used to get some insight into the hysteresis behaviour during reactive HiPIMS (R-HiPIMS). Experimental work is, however, essential and plays a critical role in the benchmarking of the simulation model. It is, therefore, surprising that dedicated experimental work on this topic is rather scarce despite the commotion after the publication of the paper by Wallin and Helmersson.[1] on hysteresis free sputtering during R-HiPIMS. If only those R-HiPIMS papers are selected where the hysteresis behaviour is studied, a very limited data set (see Appendix, Table I) is obtained that makes it hard to answer the title question. Only 26 papers were found when the keyword "hysteresis" was combined with "HiPIMS" in the Web of Science. The hysteresis behaviour is discussed in some detail in 16 papers, resulting in 37 table entries of which approximately half have sufficient details to feed the simulation efforts. Two points are striking when Table I is studied in detail. First, there is a wide variety in the experimental approach to study the fundamental behaviour of reactive R-HiPIMS. Different ways of powering make comparison difficult. Second, the number of reactive gas/target material combinations is limited. Most papers focus on Ti/O_2 and Al/O_2 (28 of 37 entries) with a few interesting exceptions. A possible reason for this scarcity is the difficulty to perform a hysteresis experiment during R-HiPIMS. This is already mentioned in the paper by Wallin and Helmersson. who mentioned that arcing can be an issue during R-HiPIMS and hence limits the parameter space that can be accessed. In Wallin's paper, this limit affects even the validity of the answer to the title question. Indeed, from this heavily dominated reactive direct current magnetron sputtering (R-DCMS) perspective, the hysteresis free behaviour discussed by Wallin *et al*. is questionable as full target poisoning was never achieved.

Another important lesson can be learned from Table I. Hysteresis during R-HiPIMS is sometimes observed. This claim has to be treated with care as the reactive gas flow is sometimes changed too fast with ramp rates up to 2 sccm/s. The observed hysteresis may then result not from the intrinsic mechanisms but from the non-steady state conditions.[2] Nevertheless, other reports on hystereses indicate that, just as in R-DCMS, the observation of hysteresis depends on the experimental conditions. So, the title question is perhaps ill-defined, and it is better to restate it as follows: It seems, although the experimental data are scarce, that it is harder to observe hysteresis during R-HiPIMS than during R-DCMS. In this perspective paper, the intension is to supply modelling based information that can give insight why this observation probability is lower.

II. THE VIEWPOINT FROM A R-DCMS MODEL

It is safe to state that the understanding of R-DCMS is more advanced than R-HiPIMS. The main reason is the longer track record of R-DCMS as discussed in Introduction, and hence, a larger amount of experimental data is available to the interested reader. The process modelling of R-DCMS started quickly after its usage to deposit compounds, and with the publication of the Berg model, it allowed to describe the process in a qualitative way.[3–5] This model describes the balance of reactive gas atoms that are consumed by the chemical reaction on the substrate and the target and by the action of the mechanical pump of the vacuum system. The target reaction results in compound formation, which finally leads to target poisoning, i.e., a strong reduction of the sputter rate. The original Berg model describes the target reaction by chemisorption of neutral reactive gas molecules.

This model is able to reproduce the S-shaped hysteresis behaviour, which is experimentally accessible by means of feedback control.[6] The existence of a hysteresis can be evaluated based on the presence of two critical points, i.e., points where the system abruptly changes as a function of an operation parameter like the reactive flow. Alternatively, the pumping speed of the system can be compared with the critical pumping speed as Kadlec et al.[7] propose. However, this approach asks from the model to resolve the unstable transition region, which will not be the case for the upcoming time-dependent models below. With this in mind, the hystereses are all simulated with time-dependent models and characterized only by their two critical points.

Latter models introduce knock-on and direct reactive ion implantation as additional target poisoning mechanisms to explain the formation of a few nanometre thick compound layers. This has led to the development of the RSD2007 (Reactive Sputter Deposition 2007) model.[8] Finally, as sputtered atoms can return to the target due to gas scattering, redeposition was added as a target process. So, as currently comprised in the RSD2013 model,[9–11] several target processes are analytically described. Moreover, the target and the substrate can be spatially resolved by the combination of the RSD2013 model with a Monte-Carlo particle-trajectory code entitled SIMTRA.[12,13] More details on the RSD2013 model and its application can be found in some recent papers.[9,14]

In this section, the RSD2013 will be applied to demonstrate some important features of the reactive sputtering process, which can give insight into the R-HiPIMS process. The system under investigation is the sputtering of Al in an Ar/O_2 atmosphere under DCMS, pulsed DCMS, and HiPIMS conditions. These conditions share the property that the periodic averaged power density is of the same magnitude (up to 50 W/cm^2), but the peak power density and as such the duty cycle are substantially different. HiPIMS is typically considered for duty cycles of <10%, while pulsed DCMS can be defined as the complement with a duty cycle of >10%, excluding of course regular DCMS with a duty cycle of 100%. The peak power density is then limited to 50 W/cm^2 for (pulsed) DCMS, while HiPIMS conditions are considered as above 50 W/cm^2 up to 10 kW/cm^2. This classification is a simplified version as the one proposed by Gudmundsson et al.,[15] as HiPIMS covers now a broader range in the peak power density. This seems justified based on Table I where several references use the term HiPIMS for these lower peak power densities.

The RSD2013 model used for the pure R-DCMS simulations is in essence the model as described by Strijckmans.[11] This simulation software[16] is freely available to the interested reader. Two solution methods are provided: a time dependent solution, which is flow controlled, or a steady state solution, which is pressure controlled. The flow controlled time dependent solution is not able to access the non-stable transition regime in contrast to the pressure controlled steady state solution. The latter solution is of course only applicable if no explicit time dependency is considered for R-DCMS. The model used here, which is further called the RSD model, is slightly adapted in the description of the deposited and redeposited reacted particles that are sputtered from the target. The compound and chemisorbed fraction on

the target, together denoted as the reacted target fraction, are still assumed to congruently sputter. This results in the definition of one molecular sputter yield for both fractions ($Y_r = Y_c$). However, in contrast to the previous version of the model,[10] it is now assumed that the formed molecules MR_z leave the target atomically as M and R atoms. This modification influences the description of the deposition on the substrate and of the (optional) redeposition on the target. In both cases, this (re)deposition means an additional metal flux and a flux of reactive gas atoms towards their surface. The metal flux increases the metallic fraction and sticks on both reacted and non-reacted metal sites, while the reactive atom flux sticks only on non-reacted metal sites, decreasing its number. Impinging reactive atoms unable to react are then assumed to re-enter the gas phase after recombination with another reactive atom. Two reasons motivate this modification. First, it is more realistic for the modelled Al/O_2 system that the reacted fraction is atomically sputtered.[17,18] Second, to extend this model later to account for returning ionized metal atoms, the sputtered M atoms should be treated separately from the sputtered O atoms.

It is important to mention that the ion current in the RSD model is approximated with the discharge current neglecting any electronic contribution. A changing ion-induced secondary electron emission yield Y_{isee} based on the target state is as such omitted. For the R-DCMS Al/O_2 system, this means that a relative small decrease in the ion current at fixed discharge current from the metallic to the poisoned mode is not included as the Y_{isee} is estimated as ~0.1 for Ar^+ on Al and as ~0.2 for Ar^+ on Al_2O_3,[19] under the reasonable assumption that Ar^+ remains the dominating ion species throughout the process. While this is true for R-DCMS, the situation for R-HiPIMS can be totally different. HiPIMS typically works only at higher discharge voltages compared to DCMS. It has been shown that while the Y_{isee} hardly changes for Ar^+ on Al at these higher discharge voltages, this is not the case for Ar^+ on Al_2O_3.[20] Also, the assumption of Ar^+ being the dominating ion species is violated, as metal and oxygen ionization can become comparable. However, knowledge of all these individual Y_{isee}s is rather scarce or not existing. The importance of the electronic contribution will depend on the target material/reactive gas combination under investigation. For a Ti/O_2 system, for example, IR modelling[21] shows that its impact is low, which seems to be in line with the limited increase in the Y_{isee} as a function of the discharge voltage for both its metal and its oxide.[20]

The RSD model for R-DCMS is extended to a RSD^{+P} model to allow a time dependent current, which is needed to include the most important feature of HiPIMS, namely, the high current pulses. This RSD^{+P} model permits for a time dependent current. Due to this inherent time dependency, only the time-dependent solution of RSD can be applied. Based on this RSD^{+P} model, two additional versions RSD^{+PR} and RSD^{+PM} were established. Each version accounts for a separate additional effect, which is claimed to be important during R-HiPIMS. The RSD^{+PR} model accounts for a lower sticking coefficient of the reactive gas during pulse-off-time, compared to pulse-on time.[22] The RSD^{+PM} model includes the implantation of an ionized

sputtered metal during the pulse-on time. As no plasma model is included, the fraction of the sputtered metal that ionizes and gets implanted becomes an additional parameter. The implementation of the RSD^{+P} and RSD^{+PR} is rather straightforward due to the possibility to describe the dynamics of reactive sputtering with the RSD model. For the RSD^{+PM}, some extra commenting is at place. The RSD model includes already the implantation of reactive ions, which is described by a Gaussian implantation profile. The metal implantation profile is also described in a proper way by a Gaussian. However, the assumption that implanted species do not occupy additional volume within the target is already disputable for the implantation of oxygen in aluminium. To illustrate, the Al number density in stoichiometric Al_2O_3 decreases already by $\sim$20% compared to pure Al. If implantation of Al also is accounted for, this is even further violated. As such, the RSD^{+PM} model accounts for the volume expansion by metal implantation. It includes homogenous relaxation terms within the equations of the target, based on the study by Sigmund and Lam.[23] Volume expansion by implanted oxygen is, however, not yet included.

The independent parameters where the RSD model relies on are summarized in Table II for the reference Al/O_2 system. The parameter choice is partially based on the fitting results of this kind of system[24] for a one-cell (uniform) description of the target. This ensures that the reference Al/O_2 system is parametrized with some level of realism. Nevertheless, the goal of the presented simulations is not to quantitatively match some experimental hystereses but to show some well-chosen trends influencing the hysteresis behaviour related to the title question. All simulations with the RSD model, and the described extensions, are set-up from this reference system at the same averaged power of 100 W, unless otherwise mentioned. A rectangular block pulse is used in the extensions. To keep the averaged power constant, the current is increased when the duty cycle is lowered at fixed frequency. Note that the chosen substrate area can be somehow considered l as it should embody all gettering surfaces in a typical vacuum system. This results in a relative higher pressure at the first critical point compared to most experiments. Realistic chamber geometries and deposition profiles can be included based on SIMTRA[13] simulations. However, we chose to restrict the modelled system to its essentials, avoiding unnecessary details complicating the picture.

In Section II A, the influence of the argon pressure on the hysteresis during DCMS is investigated with the RSD model. Section II B shows with the RSD^{+P} model the sputter cleaning of an oxidized target. Also, the hysteresis behaviour due to a current pulse with a varying duty cycle is studied with the RSD^{+PR} model. Finally, in Section II C, the important effect of metal implantation is treated from a DCMS viewpoint with the RSD model by the effects of redeposition and an effective reaction rate coefficient. This is then compared with the RSD^{+PM} model including metal implantation.

A. The influence of the argon pressure

Quite often, the working gas pressure during R-HiPIMS is higher as compared to similar experiments in R-DCMS.

Probably, the most important reason for this higher pressure is related to the delay of the current rise. It has been reported that this delay time became long when the pulse frequency was decreased,[25] the discharge voltage lowered,[26] and the working pressure reduced.[27,28] To avoid the extinguishing of the plasma and/or to allow the discharge current to substantially increase, i.e., at the characteristic high peak currents for HiPIMS, the working pressure is on average higher under HiPIMS conditions as compared to DCMS. At this point, it is also interesting to remark that most experiments described in the overview table (see Appendix, Table I) use a large target. The magnetron discharge stability is typically higher for bigger systems.

Changing the working pressure in a R-DCMS system has several impacts. The discharge voltage as the effective erosion zone (racetrack) decreases for increasing working pressure (at a fixed current), at higher working pressure, gas rarefaction becomes more prominent, and the deposition and redeposition of sputtered material change. Of course, all these effects impact the hysteresis.[11] Here, the effect of redeposition is discussed in Section II C, while gas rarefaction is touched on in Section II B. In this section, the diluting effect of an increasing working pressure on the reactive gas fraction is treated. This effect of the working gas pressure during R-DCMS was demonstrated by Sarhammar et al.[29] They showed that it primarily attributes to the disappearance of the hysteresis at higher working gas pressures for some target material/reactive gas combinations and especially for the Al/O_2 combination. The RSD model permits to assist in the understanding of this behaviour. Figure 1 shows the oxygen fraction, i.e., the oxygen pressure vs. the total pressure, as a function of the oxygen flow for a low (Figure 1(a)) and a high (Figure 1(b)) sticking coefficient of the reactive gas on the target. The other simulation parameters were kept constant (see Appendix, Table II).

For a low sticking coefficient (see Figure 1(a)), the hysteresis clearly vanishes at higher working pressure, while for the high sticking coefficient case (see Figure 1(b)), hysteresis is still observed at higher pressure. This difference in behaviour is related to the two included target processes, i.e., chemisorption and direct ion implantation. Chemisorption is defined by the oxygen flux towards the target, i.e., the process is influenced by the oxygen pressure. For ion implantation, the oxygen fraction is of importance because the oxygen ionization probability depends on the fraction in the plasma. So, when the argon pressure is increased, the balance between both processes will shift towards more chemisorption. To poison the target by increasing the oxygen flow, it is clear from Figure 1 that higher oxygen fractions are needed for a low target sticking coefficient because target poisoning is mainly driven by ion implantation. Chemisorption becomes more important if the argon pressure increases. This results in two effects. First, the target poisons at lower oxygen fractions but at higher oxygen pressures (not visible in Figure 1). This means that more oxygen needs to be introduced to poison the target, and hence, the first critical point shifts to the right. This effect is much less pronounced for a high target sticking coefficient as the target is mainly poisoned by chemisorption. Second, on returning from the
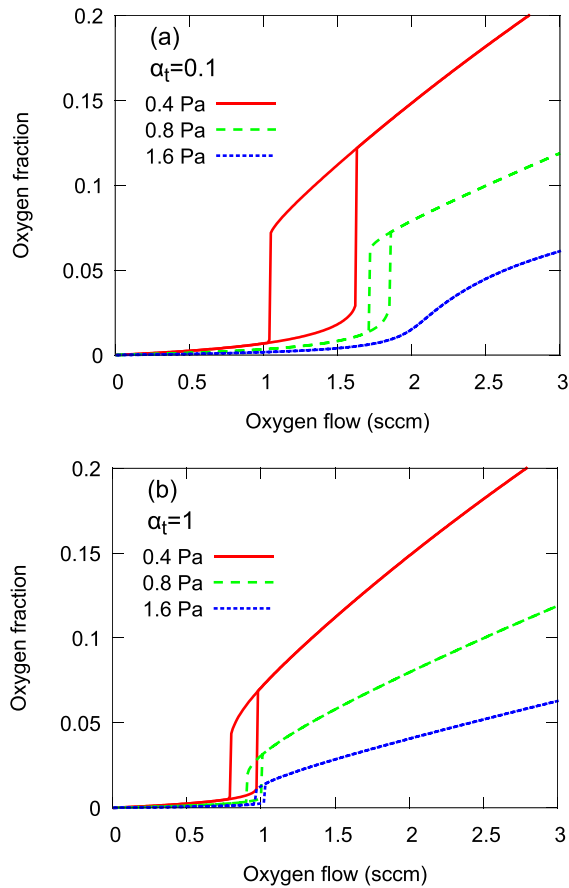
FIG. 1. Simulated hysteresis behaviour at different working pressures. The figure shows the oxygen fraction, i.e., the ratio of the oxygen pressure vs. the total pressure, as a function of the oxygen flow. Both figures have been simulated with the standard parameters, except for the sticking coefficient of the reactive gas on the target. For the top figure (a), the sticking coefficient was set to 0.1, while a value of 1 was used for the bottom figure (b).

poisoned mode, i.e., at the second critical point, target poisoning is mainly defined by ion implantation as chemisorption on a highly oxidized surface is limited, and the oxygen fraction is high. However, when the argon pressure is increased, again chemisorption takes over. This is nicely demonstrated by the shift to higher oxygen flows of the second critical point in both cases. As one poisoning mechanism is "switched off," it becomes easier to return to the metallic mode. The difference between the high and the low sticking coefficient behaviour will be amplified when the sticking coefficient on the substrate is changed, which is proportional to the change of the target sticking coefficient. The rather artificial conditions, i.e., a high sticking coefficient on the target but a low one on the substrate, were just used to explain the effect.

One of the often studied target material/reactive gas combinations in R-HiPIMS, i.e., Al/O_2, belongs to the low sticking coefficient case as demonstrated by Sarhammar et al.[29] Also, for another often studied target material/reactive gas combination, i.e., Ti/O_2, the hysteresis can easily be removed when the argon pressure is locally increased in R-DCMS.[30] As the knowledge is dominated by experiments with Ti and Al in O_2/Ar, these two findings indicate that perhaps just the fact that HiPIMS works quite often at higher

working pressures is sufficient to lower the probability to notice a hysteresis effect.

B. High current pulses

HiPIMS uses in contrast to DCMS high current pulses. The RSD^{+P} model implements these high current pulses. The effect of the duty cycle and the frequency was studied in detail. The frequency ranged from 1 Hz to 1 kHz, while the duty cycle ranged from 5% to 80% at a constant average power of 100 W. No effect on the hysteresis was observed, except for the lowest frequency of 1 Hz. This behaviour was already reported by Berg and Nyberg.[4] The reason is that the reaction kinetics during reactive magnetron sputtering are much slower as compared to the generally used pulse frequencies for R-HiPIMS. From this viewpoint, the process runs almost independently of the frequencies. The use of low frequency current pulses was experimentally explored by Billard and co-workers.[31–35]

Another effect that is claimed to influence the hysteresis during R-HiPIMS is the enhanced target cleaning (e.g., removal of oxide layer) during the pulse-on time due to the high current pulse. Of course, similar to R-DCMS, the sputter cleaning of the target will be more effective with increasing average power. This is illustrated in Figure 2. The target is first poisoned by the introduction of 8 sccm of oxygen for 5 s (see grey region). The time to poison the target, i.e., to reach a metal fraction θ_m equal to zero, depends on the power. Then, the oxygen flow is switched off, and the cleaning of the target is followed until the target is again completely metallic ($\theta_m = 1$). The time to clean the target scales inversely with the power. If now the R-DCMS simulations are compared with the RSD^{+P} simulations for the R-HiPIMS case, it is noticed that the target only poisons noticeably slower at the highest power during R-HiPIMS and that there is only a minor effect on the target cleaning. For the RSD^{+P} simulations, the peak current is fixed, but the duty cycle is accordingly increased corresponding to the increasing DC powers. The frequency is set at 1 kHz. From
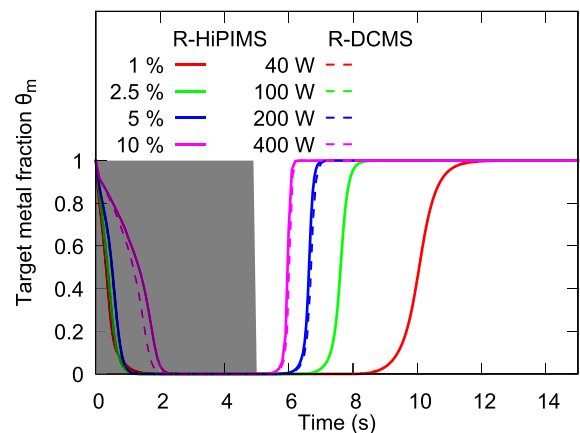

FIG. 2. The poisoning and sputter cleaning dynamics of the Al target. First, the target is poisoned by the addition of an oxygen flow of 8 sccm for 5 s (see grey area). The R-DCMS and the R-HiPIMS cases are compared at the same average power. The power increase is obtained in the R-DCMS case by an augmentation of the current, while in the R-HiPIMS case by an increase in the duty cycle.

these simulations, it is clear that the time to clean a poisoned target is of the order seconds, which is at least an order of magnitude longer than typical pulse periods (10^{-1} to 10^{-4} s).

An effect that was not considered here is that the high peak power within the pulse implies a much higher discharge voltage compared to R-DCMS. This increased discharge voltage amplifies the oxide sputter yield, which would enhance cleaning. However, it is the product of the current and the sputter yield that defines target cleaning or the oxide erosion rate. When the same product of the current and the voltage, i.e., power, is used for both the R-DCMS and the R-HiPIMS, the oxide erosion rate will be unaffected *if* the sputter yield linearly scales with the voltage. This relation is, however, not well known for Al_2O_3. The experimental data are scarce,[36] while a simulated relation is suggested by Depla *et al.*[9] In the latter, a slight supralinear relation was found for the relevant voltage range, which indicates that sputter cleaning would be slightly more effective in R-HiPIMS due to the higher used voltages.

During the R-HiPIMS pulse, reactive gases such as nitrogen and oxygen get "activated." This activation can not only be excitation but also dissociation of the molecules. This means that during the pulse-on time, the plasma is more reactive as compared to the pulse-off time. This reactivity modulation was introduced in the RSD^{+PR} model. During the pulse-on time, the sticking coefficient of the reactive gas

is set equal to 0.1, while in the pulse-off time, it was reduced to 0.01. The selection of these values is based R-DCMS values for the measured substrate sticking coefficient[37] and the fitted target sticking coefficient obtained by modelling.[24] The pulse-off value is set equal to the average of measured sticking coefficients for molecular oxygen on Al surfaces.[38–44] Figure 3 shows the result for two pressures. The behaviour at higher pressure is somewhat surprising as the hysteresis becomes less pronounced at higher duty cycles, i.e., at higher average sticking coefficient. In the case of the low pressure simulation (0.4 Pa, Figures 3(a) and 3(c)), the trend as a function of the duty cycle is readily understood. As the duty cycle increases, the average sticking coefficient on both the target and substrate increases. The enhanced gettering of the reactive gas results in a lowering of the oxygen pressure before the first critical point, but there is little change in the first and second critical points because the poisoning mechanism is dominated by ion implantation. The latter is not the case at higher pressure as discussed in Section II A. Indeed, the calculated chemisorption fraction (compare Figures 3(c) and 3(d)) is much higher at higher pressure, which makes chemisorption (and knock-on implantation) an important poisoning process at the first critical point. As the duty cycle is increased, the effect of ion implantation on the first critical point becomes even less important because the reactive gas fraction becomes lower
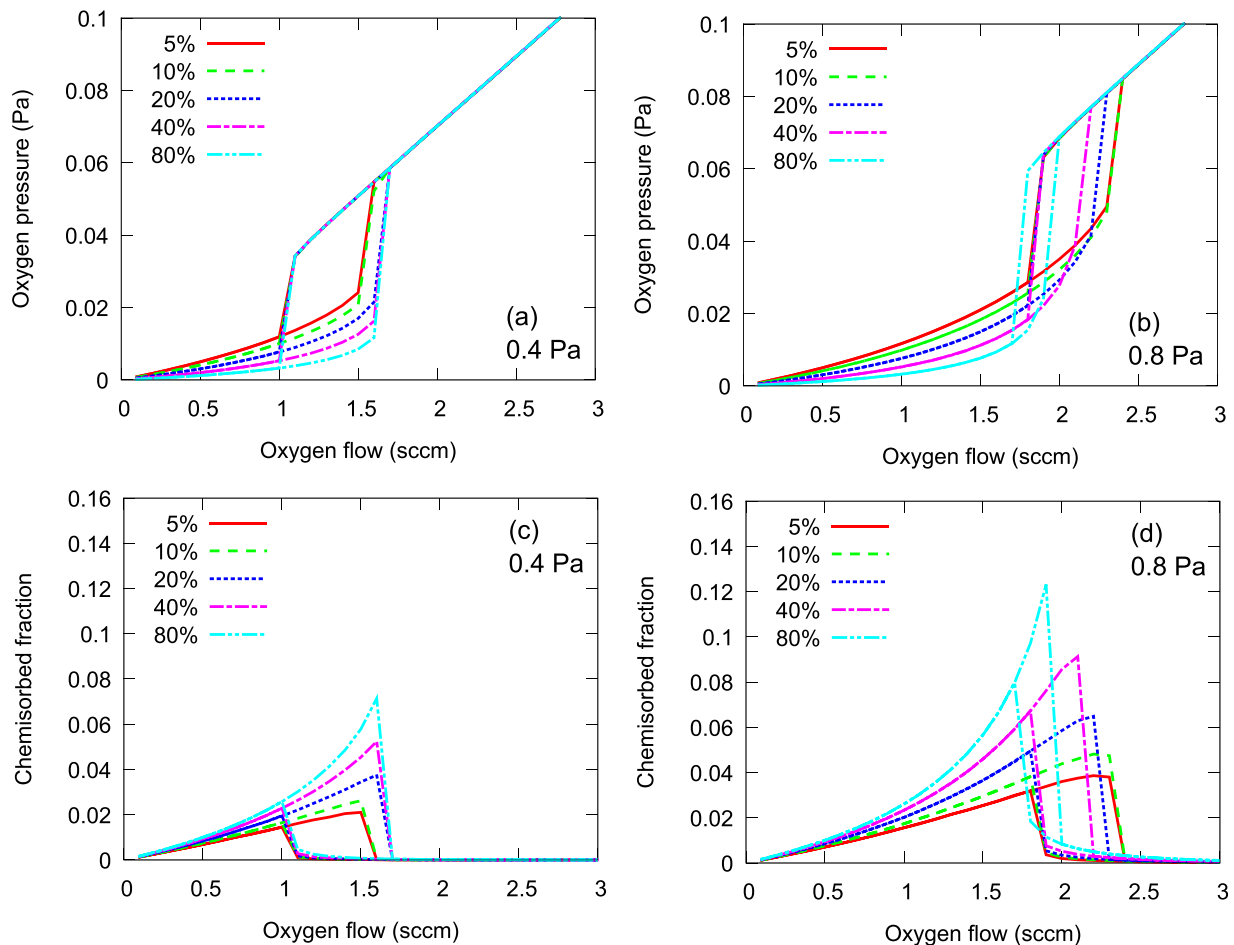

FIG. 3. The pressure hysteresis as a function of the duty cycle for argon pressures of 0.4 Pa (a) and 0.8 Pa (b). Their calculated chemisorption fractions are shown in (c) and (d), respectively.

due to the enhanced gettering. As target poisoning at the first critical point is now defined by chemisorption, this critical point shifts towards lower oxygen flows as the average sticking coefficient becomes higher. For the second critical point, which is dominated by ion implantation, due to the high oxygen fraction, a change of the sticking coefficient affects in a minor way the second critical point. The overall result is a narrower hysteresis. Although this effect is perhaps not so important in the context of the title question, it shows the subtlety of hysteresis experiments and hence the danger of making fast conclusions.

From these simulations, another conclusion can be drawn. It has been suggested that the diminishing of the hysteresis effect is due to gas rarefaction,[45] i.e., the reduction of the local gas density above the target due to the impact of the sputtered atoms with the reactive gas and the sputtering gas. The argon and oxygen gas densities can be expected to reduce in a similar way as their masses are comparable. This means that the oxygen fraction in the ion current towards the target remains the same, and therefore, gas rarefaction will probably not influence the ion implantation mechanism. A local density reduction will result in a lower reactive gas molecular flux and hence affect the chemisorption contribution to target poisoning. Chemisorption is influenced by the product of the sticking coefficient and the oxygen flux. So, it can be expected that a periodical change of the local oxygen pressure will affect the hysteresis in a similar way to a periodical change of the sticking coefficient. Despite the fact that the sticking coefficient was periodically changed between 0.01 and 0.1, i.e., over one order of magnitude, the effect on the hysteresis was small, at least in the case of aluminium. As such, this statement will also probably hold for gas rarefaction.

C. Returning metal ions

Another well-known feature of HiPIMS is the high ionization degree of the sputtered metal atoms. Due to the presence of the target bias, sputtered atoms have a given probability to return to the cathode. This feature was already recognized early after the first application of HiPIMS and was introduced in the Christie model[46] and its successors.[47,48] The influence of these metal ions on the hysteresis behaviour during R-HiPIMS was suggested by Kadlec and Capek[49] at the Reactive Sputter Deposition symposium in 2014. The influence of the recapture of sputtered atoms can be included in the RSD model in two ways. The first straightforward way is to increase the redeposition fraction in the model. Indeed, also in DCMS, sputtered atoms return to the cathode although the underlying mechanism is completely different from the HiPIMS case. In DCMS, scattering of the sputtered atoms by collisions with the working gas atoms forces, especially at higher pressures and/or for light target atoms, a given fraction of the sputtered atoms to return to the cathode. As the atoms have low energies, i.e., close to thermal, the redeposition is a surface process. Although the comparison with HiPIMS is weak, some of the returning sputtered atoms in HiPIMS could also affect the target surface condition. Therefore, in the first part of this section, the

effect of redeposition on the hysteresis behaviour will be discussed. A second way to include the recapture of sputtered atoms in HiPIMS is to change the reaction rate constant in the RSD model. The rationale behind this approach is the following: The recaptured metal atoms in HiPIMS are high energetic ions that get implanted into the target. From the viewpoint of compound formation, the addition of an extra metal to the target can be seen as a lowering of the compound formation rate in the target bulk. The influence of lowering the reaction rate constant on the hysteresis will be studied in the second part of this section. Finally, in the last part of this section, the effect of metal ion implantation is studied. For these simulations, the RSD^{+PM} was used, which was described at the beginning of Section II.

The effect of an increased redeposition fraction on the hysteresis behaviour is shown in Figure 4. A clear shift of the first critical point towards lower oxygen flow is observed. This shift can be understood from the lower getter capacity of the process. As less metal is deposited on the substrate and the chamber walls, less reactive gas can be consumed by the substrate. Therefore, the target poisoning occurs at lower reactive gas flow. As Figure 4 shows, not only the first critical point but also the second critical point shifts in a minor way. Redeposition on the target results in a lower effective erosion rate that is defined by the action of both the sputter and the redeposition rate. When reactive ion implantation is the major poisoning mechanism, i.e., at the second critical point, the erosion rate defines the allocated time for the implanted reactive ions to react with the target material. When the redeposition fraction increases, and subsequently the erosion rate decreases, more compounds will be formed between the moment of implantation and the arrival of the implanted atom at the target surface. It becomes therefore more difficult to return to the metallic mode. As a result, together with the first critical point, also the second critical point shifts towards lower oxygen flows.

Figure 5 shows the hysteresis behaviour of the oxygen partial pressure as a function of the oxygen flow for 4 different reaction rate constants. Clearly, when the reaction rate
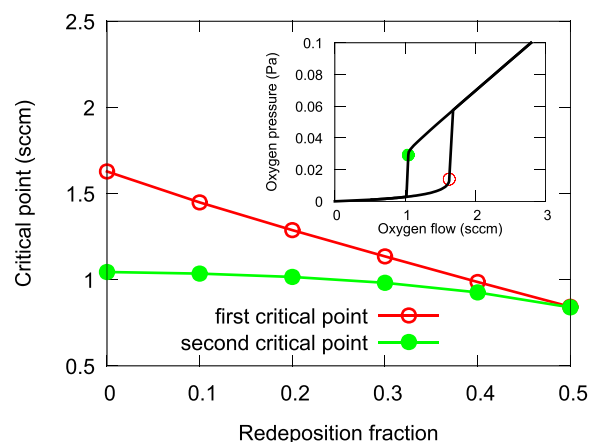
FIG. 4. The critical points as a function of the redeposition fraction. The inset shows the pressure hysteresis for the "standard" conditions. The two indicated points are the first (open marker) and the second (closed marker) critical point. Above a redeposition fraction of 0.6, no hysteresis was observed.
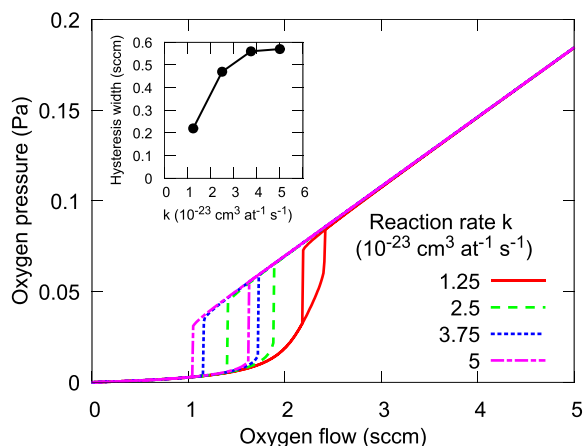
FIG. 5. The simulated hysteresis behaviour of the oxygen pressure as a function of the oxygen flow for different reaction rate constants of the implanted oxygen in an aluminium target. The other simulation conditions were set equal to the "standard" conditions as in Table II.

constant is lowered, the hysteresis effect becomes less pronounced. It is perhaps too simple to state that the reaction rate constant scales inversely with the return probability (see further). However, it is clear that a 50% reduction of the reaction rate already results in 18% reduction of the hysteresis width. For 75% reduction of the reaction rate, the effect is even stronger (62% reduction of the hysteresis width, see inset). Therefore, it is safe to state that the implantation of metal ions balances the chemical reaction towards a more metallic target at the same oxygen flow.

Finally, the effect of metal ion implantation is studied for both R-DCMS and R-HiPIMS (see Figure 6). The effect is very similar for both powering methods and confirms in this way the discussion given above. When the metal return probability is increased, less metal is used in the chemical reaction on the substrate. Therefore, the hysteresis shifts towards lower oxygen flows as discussed in connection with the redeposition process (see Figure 4). However, in contrast to the simulation including only redeposition, both critical points strongly shift. This behaviour shows that redeposition alone cannot explain the hysteresis reduction in R-HiPIMS and that the simulation result shown in Figure 4 is mainly due to the reduced getter capacity. Indeed, the linear behaviour between the first critical point and the redeposition fraction shows a strong resemblance with the effect of lowering the deposition rate as discussed by Depla *et al.*[9] The shift of both critical points corresponds to the effective lower reaction rate for compound formation as the metal implantation balances the compound formation as discussed in the context of Figure 5. As such, Figure 6 can be seen as a combined effect of metal redeposition and a reduced reaction probability.

III. TOWARDS A R-HIPIMS MODEL

In Section II, several important effects for the hysteresis behaviour during R-HiPIMS were investigated from the viewpoint of R-DCMS modelling and extensions of this model towards the HiPIMS situation. It is concluded that ionization and implantation of sputtered metal play a key
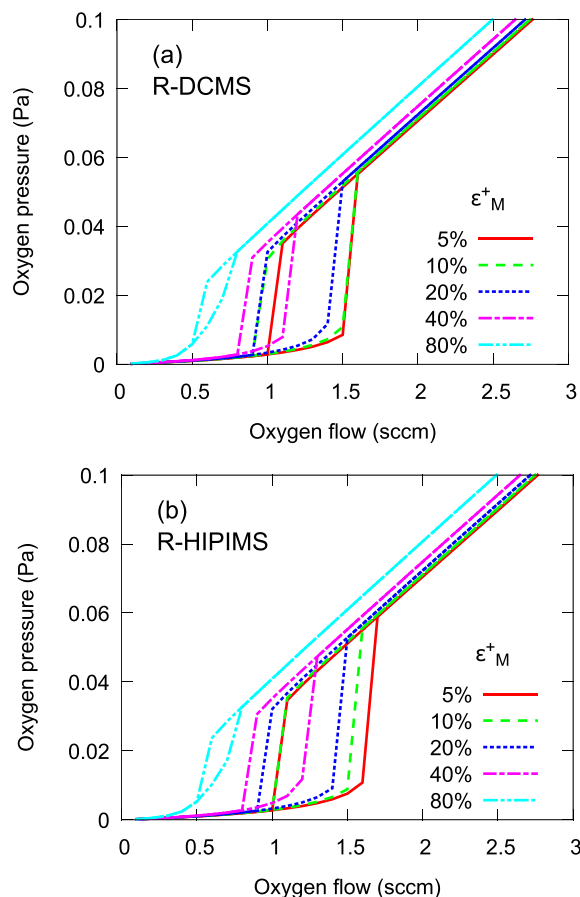

FIG. 6. The influence of the combined ionization and return probability of a sputtered metal ε_{M^+} on the hysteresis behaviour during (a) R-DCMS (duty cycle 100%) and (b) R-HiPIMS with duty cycle 10%. A frequency of 1 kHz was used for the R-HiPIMS configuration, while the argon pressure was 0.4 Pa in both cases.

role in answering the title question. Notwithstanding, the RSD^{+PM} model describes this effect, and it depends on the input parameter ε_{M^+} that stands for the ionization and returning probability of sputtered metal. To quantify this parameter, the need of coupling the RSD model with a plasma model emerges. Such a plasma model would have the advantage that also other plasma related effects and details can now be included that are missing in the RSD model. Indeed, in the RSD model, it is assumed that the flux of reactive ions implanted into the target is proportional to the ratio of the partial reactive pressure to the total pressure. This neglects any difference in ionization probability between the reactive and inert gas particles. Such and other plasma details can be expected to have a larger influence on the reactive behaviour during R-HiPIMS compared to R-DCMS. In the study by Raadu *et al.*,[50] the ionization region model (IRM) was proposed to describe the non-reactive HiPIMS plasma for the sputtering of Al. This basic model was further improved[50–53] to better describe the plasma conditions. Recently, a R-IRM[21] was proposed to simulate the R-HiPIMS plasma. This plasma model seems at this moment the right candidate to couple with a reactive sputter deposition model because of two main reasons. As the IR model is a time-dependent global (volume averaged) model for the plasma chemistry defined by rate equations in the form of ordinary differential

equations, it has a low complexity. This has the advantage that an acceptable fast simulation is possible. This is a necessary condition as the timescale to correctly resolve the HiPIMS pulse-on time is of the order 10^{-6} s. This contrasts the timescale on which the reactive behaviour stabilizes to the steady state, which is of the order seconds as shown in the discussion on sputter cleaning (Figure 2). Luckily, the duty cycle of HiPIMS is typically <10% and repetition frequencies <10 kHz, which allows the integration step during pulse-off time to increase to at least a factor of 10. Furthermore, the IR model accounts not only for the plasma chemistry but also for several transport effects. Gas rarefaction is here of particular interest as it is claimed another coined effect to explain hysteresis reduction.[45] Finally, the IR model has been connected with some experimental results at least for the non-reactive case.[54]

A. RSD^{+IR} model

The strategy is now to integrate the basic reactive IR model into the RSD model. The starting point was the non-reactive IR model proposed by Raadu et al.[50] where now the reactive species were added. In this first approach, the extra included species were kept to a minimum. Only ground state molecular and atomic oxygen and their first positively ionized states were added besides an atomic "hot" oxygen component that originates from oxide sputtering. Most input data such as reaction rates, sputter yields, and cross-sections for the non-reactive species are taken from the paper by Raadu et al.[50] For the reactive species, the paper by Gudmundsson and Thorsteinsson[55] is a useful source. Concerning the simulated Al/O$_2$ system, the current-voltage data for metallic and poisoned mode and system configuration published by Aiempanakit et al.[56] are used. In more detail, the described setup is a two inch Al target sputtered in an Ar pressure of 0.8 Pa (pumping speed ~50 l s^{-1}) at a frequency of 500 Hz and a pulse length of 50 μs. Both metallic and poisoned modes were maintained at a constant average power of 50 W.

A schematic of the coupling between the IR model and the RSD model is given in Figure 7. The two models run simultaneously where the time step is dictated by the much faster dynamic of the plasma. Every time step, parameters between the two models are exchanged. The RSD model supplies the state of the target by its metal (θ_m) and reacted ($\theta_r + \theta_c$) fraction, the global reactive P$_{O_2}$ and the fixed inert P$_{Ar}$ partial pressure in the chamber, and the desorption flux F$_{O_2}$ of non-reacted implanted reactive gas ions due to sputter erosion as recombined molecular oxygen. The reactive partial pressure P$_{O_2}$ still determines the reactivity at the substrate side and the diffusional refill of the IR. This IR is spatially separated from the target surface by a sheath thickness. However, this distance is considered sufficiently small (~mm) to reasonably assume that the particle fluxes that leave the IR hit the target unchanged. As such, the IR is
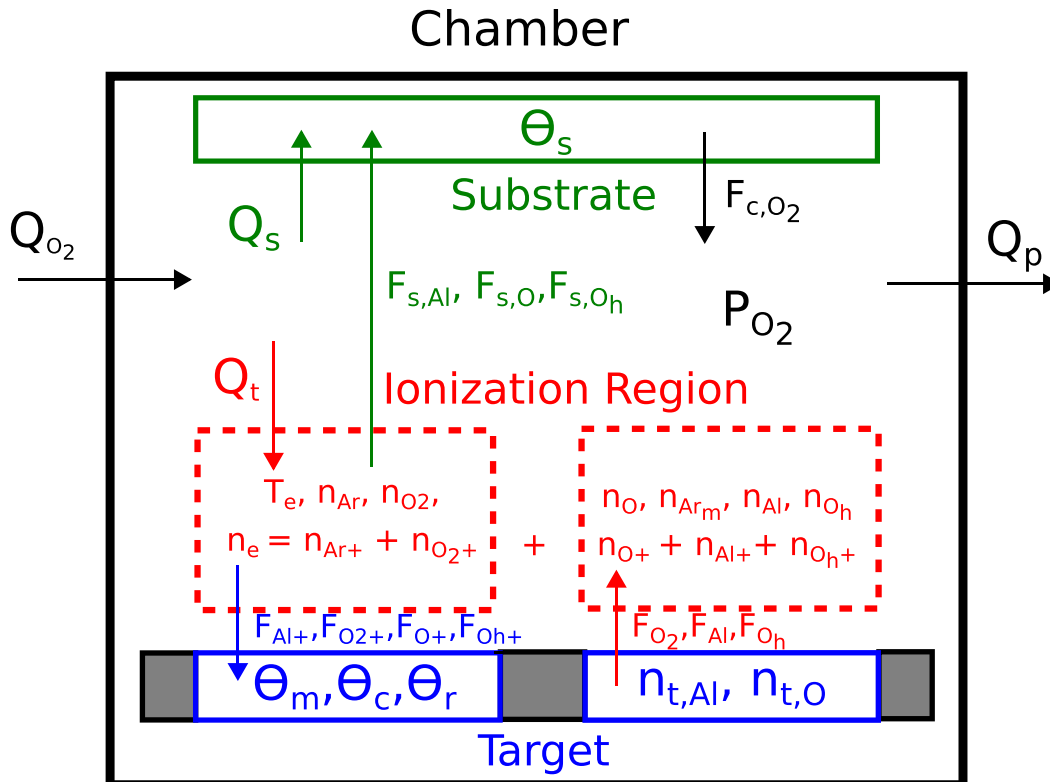

FIG. 7. Schematic of the coupling between the RSD and the IR model. The RSD model is subdivided in the chamber with partial reactive pressure P$_{O_2}$, the substrate with compound fraction θ_s and the target with metal fraction θ_m, chemisorbed fraction θ_c and compound fraction θ_r at the surface, and concentrations of the non-reacted metal n$_{t,Al}$ and non-reacted oxygen n$_{t,O}$ in the bulk. The IR model solves for the densities n$_x$ of the relevant species x and the electron temperature T$_e$. The electron density n$_e$ is based on the quasi-neutrality condition. Both models are coupled by in- and outgoing fluxes F$_x$ of particles together with the molecular oxygen flow balance (Q$_{O_2}$, Q$_t$, Q$_s$, and Q$_p$) of the RSD model. Any transport of Ar is omitted in the figure. More details of the individual models can be found in the study by Raadu et al.[50] and Strijckmans and Depla.[10]

virtually in direct contact with the erosion zone of the target and defines in this way the ionic and reactive fluxes that modify the state of the target. In the opposite direction, the sputtered species leaving the target first enter the IR where they can be modified due to plasma interactions. They also form the sputter wind[57] that causes some gas rarefaction in the IR. The particles that leave the target define the oriented sputtered particle fluxes of metal and reactive particles towards the substrate or the deposition flux. The metal particles are fully incorporated into the growing film. For the reactive particles, the incorporation will depend on the available non-reacted metal sites. If these reactive particles do not find a metallic reaction partner on the substrate, they are assumed to desorb as molecular gas (see flux $F_{c,O2}$ on Figure 7). This then increases the global reactive partial pressure P_{O2}.

The current-voltage-time (IVt) characteristic forms an essential input for the IR model. The experimental IVt characteristic is fitted with a single parameter F_{PWR}.[50] This fit parameter F_{PWR} represents the fraction of the electrical power used to heat the electrons. As the operation mode, i.e., metallic or poisoned, strongly defines the IVt characteristic,[56] it is necessary to modify the IVt characteristic for the changing target condition in the model. Starting from the experimental IVt for the pure metallic and poisoned states, the intermediate states are calculated by linear interpolation as a function of the target state. The experimental input IVs for both operation modes are first individually fitted with the single parameter F_{PWR} (0.40 for the metallic mode and 0.31 for the poisoned mode). Similarly, as the IVts, this parameter is linearly interpolated for the intermediate states.

B. First result

A hysteresis during R-DCMS and R-HiPIMS has been simulated with the RSD^{+IR} model (see Figure 8). To allow some level of comparison with the previous RSD and modified RSD simulation results (see Section II), the average power of 100 W is taken in both the R-DCMS and the R-HiPIMS simulations. A frequency of 1 kHz was used in
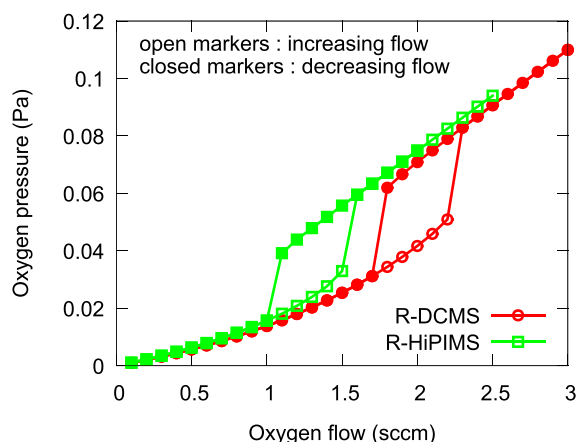

FIG. 8. RSD^{+IR} simulation of the Al/O$_2$ hysteresis in the R-DCMS regime and in the R-HiPIMS regime at the same average power of 100 W for an argon pressure of 0.8 Pa. The experimental IVt-characteristic and configuration were taken from the study by Aiempanakit et al.[56] for the R-HiPIMS case. Only the frequency was increased to 1 kHz.

the R-HiPIMS simulations. Remark that now the hystereses are simulated at constant power, while the previous modified RSD simulations were at constant current. Considering this, the metallic mode towards the first critical point ran under comparable power conditions in the constant current mode, while the poisoned mode towards the second critical point ran under lower power conditions ($\sim$70 W) due to the lower discharge voltage in the poisoned mode. For the RSD^{+IR} simulation of the R-DCMS regime, the discharge voltages and currents are interpolated between the metallic mode (350 V, 0.286 A) and the poisoned mode (250 V, 0.4 A), maintaining the constant power of 100 W.

In both cases, a clear hysteresis is observed in Figure 8, but for the R-HiPIMS conditions, a substantial shift of the whole hysteresis to lower oxygen flows is observed. This can be explained based on the increased return probability of the sputtered metal that ionizes and is back attracted, like treated in Section II C. Indeed, this return probability ε_{M^+} for the R-HiPIMS case is around $\sim$20% during the metallic mode, while for the R-DCMS case, it settles around $\sim$10%. From this first result, almost no diminishing or vanishing of the hysteresis is observed, only a shift. This observation seems to be in line with the results from Section II C. If the return probability is rather modest ($<$40%), no strong diminishing of the hysteresis is observed. However, the return probability ε_{M^+} is now likely underestimated due to the used IR model. In this basic version,[50] the generated ions have no preferred direction of leaving the IR. It is implicitly assumed that no potential difference exists over this region and that the full potential fall is over the sheath outside the IR. More recent versions of the model[21,51–53] acknowledge this and modified the model to establish a small part of the potential fall over the IR, coupled with an additional back attraction probability towards the target with a value close to unity.[21] This would greatly enhance the return of ions by some factor of two. If this is the case, a much stronger effect of returning and implanted metal ions may be expected, which would result in a diminishing of the hysteresis according Figure 6. This first result indicates that the prime effect of R-HiPIMS on the hysteresis is probably the returning of metal ions. The IR model for Al/O$_2$ eliminates also the effect of gas rarefaction as a possible mechanism for hysteresis reduction. Indeed, in the case of Al/O$_2$, gas rarefaction is mainly caused by the ionization and the attraction towards the target of the gas species.[50] This means that the reactive gas is more efficiently, as compared to R-DCMS, attracted to the target. The same conclusions, both for metal ion implantation and gas rarefaction, were obtained based on the simulations in Section II from a more DCMS viewpoint.

IV. CONCLUSIONS

An often claimed experimental observation for R-HiPIMS, i.e., the hysteresis reduction, is carefully inspected from a R-DCMS viewpoint. From the limited amount of available experimental data, this statement seems to hold. Based on a modified R-DCMS model, it becomes clear that gas rarefaction, enhanced target cleaning, and the activation of the reactive gas by the high density plasma can be ruled

out as possible mechanisms for the hysteresis reduction. Sputtered metal atoms that become ionized and return to the target seem to be the most important mechanism. This effect is not a pure surface process as a clear difference between the effect of metal redeposition and of metal implantation in R-DCMS is observed. The metal implantation reduces the overall compound formation in the bulk target. To improve the R-DCMS model, the RSD2013 model was coupled with the global ionization region model. Preliminary results seem to confirm the above hypothesis. However, it also indicates

the necessity of a more profound IR model for simulating R-HiPIMS deposition than the model used here. This point, in combination with the need for more experimental work on this topic, shows that the R-HiPIMS has a bright future, but as stated by Niels Bohr,[58] "Prediction is very difficult, especially if it is about the future."

APPENDIX: EXPERIMENTAL DATA AND MODEL PARAMETERS

TABLE I. Experimental data on hysteresis behaviour during R-HiPIMS.

References	Target[a] (mm)	Reactive gas	S^b (l/s)	DC^c	$P_{Ar}{}^d$ (P_{tot})	ν^e (kHz)	Duty cycle (%)	Power density (W/cm^2)	Peak power (W/cm^2)	Power	Remarks
59	Zr (76)	O$_2$		Yes	0.8 Pa	2	11.1	~4	35.4	Average pulse current 0.6 A	
						0.67	3.33		120.1	Peak current 5.8 A	
1, 60	Al (50)	O$_2$		Yes	0.8 Pa	1	3.5			600 to 800 V, 7 to 25 A	HiPIMS stopped before full poisoning,
61	Ti (188 × 296)	O$_2$	50		0.5 Pa	0.3	1.5	~5.4	360	3 kW, 920 V	Fast ramping of oxygen flow (2 sccm/s)
						0.45	2.25		240	3 kW, 789 V	Hysteresis observed
						0.6	3		180	3 kW, 750 V	
62, 63	Ti (188 × 296)	O$_2$		Yes	1 Pa	0.325	1.625	~4.5	277	2.5 kW, 900 V	Fast ramping of oxygen flow (2 sccm/s) Hysteresis is observed
64	Cr (188 × 296)	O$_2$/CO$_2$/C$_2$H$_4$			0.2 Pa	0.6	3	~5.4	180	3 kW, fixed voltage	Fast ramping of oxygen flow (2 sccm/s)
	Al (188 × 296)	O$_2$									Hysteresis is observed
	Zn/Al (188 × 296)	O$_2$				0.06	1.2	~1.8	150	1 kW, fixed voltage	
45	Ti (100)	O$_2$	42		0.8 Pa	0.5	2.5	~5.1	204	0.4 kW, fixed voltage	Hysteresis is observed
						1	5		102		Normalized oxygen flows are given
						2	10		51		
65	Al (50)	O$_2$	20	Yes	0.8 Pa	1	3.5	~5.1	146	Fixed voltage and power	Power is adjusted when frequency is changed
						2	7		73		
						4	14		38		Power density is for DC
	Al (50)	O$_2$	20	Yes	0.9 Pa	2	7		146		Higher power as first series of experiment
						4	14		73		Power is adjusted when frequency is changed
						10	35		38		
	Ce (50)	O$_2$	25	Yes	0.65 Pa	1	7	~3.6	146	Fixed voltage and power	Power is adjusted when frequency is changed
						2	14		73		
						4	35		38		Power density is for DC
66	Nb (50)	O$_2$	75	Yes	1 Pa	0.05	10	~16.3	163	1200 V; 320 W (metal mode)	
67	Ti (450 × 150)	O$_2$	320	Yes	0.5 Pa			~6		1000 V, 4000 W, 160 A	Varied frequency to obtain constant peak current
										1000 V, 4000 W, 300 A	
										1000 V, 4000 W, 400 A	Hysteresis is observed in all cases.
										1000 V, 2000 W, 400 A	
68	Ti 305 × 120	O$_2$		Yes	0.6 Pa	0.2	1	~5.3	530	600 V, 2 kW	
						0.5	2.5		140	600 V, 2 kW	
69	Si (100)	**O$_2$**	253		0.3 Pa	1	4	~0.5	12.5	1000 V (40 W, metallic mode)	

TABLE I. (*Continued.*)

References	Target[a] (mm)	Reactive gas	S[b] (l/s)	DC[c]	P_{Ar}[d] (P_{tot})	ν[e] (kHz)	Duty cycle (%)	Power density (W/cm²)	Peak power (W/cm²)	Power	Remarks
	Ta (100)	**O₂**	253			1	4	~10	250	1000 V (800 W, metallic mode)	
70	Al (100)	O₂			0.66 Pa	10	10	~5	50	660 V, 400 W	Hysteresis is observed
						4	10	~9	90	500 V, 700 W	
71	Hf (76.2)	N₂			0.4 Pa	0.6	1.5	~2.6	173	450 V (120 W in metallic mode)	
72	Cr (600 × 200)	N₂	1013		0.33 Pa	0.1	2	~6.7	335	8 kW	Fast ramping of the reactive gas flow (0.25 sccm/s)
73	Ti (50)	O₂	25	Yes	1 Pa	0.2	2	~10.2	510	25–35 A, 200 W	
			25				0.4	4		255	25–35 A, 200 W
74	V (50)	O₂	70		1.3 Pa	0.2	0.9	~15.3	1700	900 V, 300 W	

[a]A single value denotes the radius of a circular target, while the length and width are given for rectangular targets.
[b]Pumping speed.
[c]If a hysteresis during R-HiPIMS is compared with a hysteresis under direct current (DC) conditions.
[d]Working pressure of argon (normal font) or the total pressure (italic font).
[e]Pulse frequency.

TABLE II. Description of the parameters used in the RSD, RSD[+P], RSD[+PR], and RSD[+PM] models.

Parameters	Value	Description
RSD		
Y_m [#M(R_z) ion⁻¹]	0.756	Sputter yield of metal atoms M
Y_r, Y_c [#M(R_z) ion⁻¹]	0.06	Sputter yield of compound molecules MR_z, chemisorbed molecules MR_z
α_t	0.1	Sticking probability of reactive gas on metal for target
α_s	0.1	Sticking probability of reactive gas on metal for substrate
K [cm³ s⁻¹ #M(R_z)⁻¹]	5×10^{-23}	Reaction rate coefficient of implanted reactive atoms with metal particles
β [#R ion⁻¹]	0.2	Knock-on yield of chemisorbed reactive atoms
$p(x)$ [cm⁻¹]	R_p=1.4 nm	Mean of Gaussian implantation profile of reactive atoms
	dR_p=0.8 nm	Deviation of Gaussian implantation profile of reactive atoms
n_0 [#M(R_z) cm⁻³]	6.03×10^{22}	Particle density
z	1.5	Stoichiometric factor
I [A]	0.286	Discharge current
P_i [Pa]	0.4	Inert working gas pressure
T [K]	300	Gas temperature
V [cm³]	12 500	Volume of vacuum chamber
A_t [cm²]	10	Area of target
A_s [cm²]	1000	Area of substrate
S [l s⁻¹]	48.54	Gas pumping speed
RSD[+P]		
I [A]	5.7, 2.9, 1.4, 0.71, 0.36	Discharge current in pulse
d [%]	5, 10, 20, 40, 80	Duty cycle, ratio between pulse-on-time and period
f [kHz]	1	Pulsing frequency
RSD[+PR]		
α_t, α_s	0.1 (on), 0.01 (off)	Sticking probability of reactive gas on metal during on- and off-time
RSD[+PM]		
ε_{M^+}	5, 10, 20, 40, 80	Fraction of sputtered metal flux that ionizes and is implanted
$p_M(x)$ [cm⁻¹]	$R_{p,M}$ = 1.8 nm	Mean of the Gaussian implantation profile of metal atoms
	$dR_{p,M}$ = 0.9 nm	Deviation of Gaussian implantation profile of metals atoms

[1]E. Wallin and U. Helmersson, Thin Solid Films **516**, 6398 (2008).
[2]T. Kubart, O. Kappertz, T. Nyberg, and S. Berg, Thin Solid Films **515**, 421 (2006).
[3]S. Berg, H. O. Blom, T. Larsson, and C. Nender, J. Vac. Sci. Technol. A **5**, 202 (1987).
[4]S. Berg and T. Nyberg, Thin Solid Films **476**, 215 (2005).
[5]S. Berg, E. Särhammar, and T. Nyberg, Thin Solid Films **565**, 186 (2014).
[6]W. D. Sproul, D. J. Christie, and D. C. Carter, Thin Solid Films **491**, 1 (2005).
[7]S. Kadlec, J. Musil, and H. Vyskocil, J. Phys. D: Appl. Phys. **19**, L187 (1986).
[8]D. Depla, S. Heirwegh, S. Mahieu, and R. De Gryse, J. Phys. D: Appl. Phys. **40**, 1957 (2007).
[9]D. Depla, K. Strijckmans, and R. De Gryse, Surf. Coat. Technol. **258**, 1011 (2014).

[10]K. Strijckmans and D. Depla, J. Phys. D: Appl. Phys. **47**, 235302 (2014).

[11]K. Strijckmans, Ph.D. thesis, Ghent University, 2015.

[12]K. Van Aeken, S. Mahieu, and D. Depla, J. Phys. D: Appl. Phys. **41**, 205307 (2008).

[13]D. Depla and W. P. Leroy, Thin Solid Films **520**, 6337 (2012).

[14]K. Strijckmans and D. Depla, Appl. Surf. Sci. **331**, 185 (2015).

[15]J. T. Gudmundsson, N. Brenning, D. Lundin, and U. Helmersson, J. Vac. Sci. Technol. A **30**, 030801 (2012).

[16]See www.draft.ugent.be for dowloading the RSD simulation software.

[17]J. W. Coburn, E. Taglauer, and E. Kay, Jpn. J. Appl. Phys., Part 1 **13**, 501 (1974).

[18]A. Hecq, M. Vandy, and M. Hecq, J. Chem. Phys. **72**, 2876 (1980).

[19]D. Depla, S. Mahieu, and R. De Gryse, Thin Solid Films **517**, 2825 (2009).

[20]C. Corbella, A. Marcak, T. de los Arcos, and A. von Keudell, J. Phys. D: Appl. Phys. **49**, 16LT01 (2016).

[21]J. T. Gudmundsson, D. Lundin, N. Brenning, M. A. Raadu, H. Chunqing, and T. M. Minea, Plasma Sources Sci. Technol. **25**, 065004 (2016).

[22]K. Tomas and A. Joakim, IOP Conf. Ser.: Mater. Sci. Eng. **39**, 012008 (2012).

[23]P. Sigmund and N. Lam, in *Fundamental processes in sputtering of atoms and molecules (SPUT92)*, edited by P. Sigmund (Kongelige Danske videnskabernes selskab, 1993), Vol. 43, p. 276.

[24]K. Strijckmans, W. P. Leroy, R. De Gryse, and D. Depla, Surf. Coat. Technol. **206**, 3666 (2012).

[25]A. Anders and G. Y. Yushkov, J. Appl. Phys. **105**, 073301 (2009).

[26]G. Y. Yushkov and A. Anders, IEEE Trans. Plasma Sci. **38**, 3028 (2010).

[27]J. T. Gudmundsson, J. Alami, and U. Helmersson, Surf. Coat. Technol. **161**, 249 (2002).

[28]J. Alami, J. T. Gudmundsson, J. Bohlmark, J. Birch, and U. Helmersson, Plasma Sources Sci. Technol. **14**, 525 (2005).

[29]E. Sarhammar, K. Strijckmans, T. Nyberg, S. Van Steenberge, S. Berg, and D. Depla, Surf. Coat. Technol. **232**, 357 (2013).

[30]D. Depla, J. Haemers, and R. De Gryse, Surf. Coat. Technol. **235**, 62 (2013).

[31]F. Lapostolle, T. H. Loi, A. Billard, and C. Frantz, Surf. Coat. Technol. **97**, 574 (1997).

[32]F. Perry, A. Billard, and C. Frantz, Surf. Coat. Technol. **94–95**, 339 (1997).

[33]A. Billard and C. Frantz, Surf. Coat. Technol. **86–87**, 722 (1996).

[34]F. Perry, A. Billard, and C. Frantz, Surf. Coat. Technol. **94–95**, 681 (1997).

[35]A. Billard, F. Perry, and C. Frantz, Surf. Coat. Technol. **94–95**, 345 (1997).

[36]P. D. Davidse and L. I. Maissel, J. Vac. Sci. Technol. **4**, 33 (1967).

[37]W. P. Leroy, S. Mahieu, R. Persoons, and D. Depla, Thin Solid Films **518**, 1527 (2009).

[38]A. M. Bradshaw, P. Hofmann, and W. Wyrobisch, Surf. Sci. **68**, 269 (1977).

[39]H. Brune, J. Wintterlin, J. Trost, G. Ertl, J. Wiechers, and R. J. Behm, J. Chem. Phys. **99**, 2128 (1993).

[40]D. Depla and R. De Gryse, Plasma Sources Sci. Technol. **10**, 547 (2001).

[41]P. O. Gartland, Surf. Sci. **62**, 183 (1977).

[42]C. S. Lee and T. M. Lin, Surf. Sci. **471**, 219 (2001).

[43]L. Osterlund, I. Zoric, and B. Kasemo, Phys. Rev. B **55**, 15452 (1997).

[44]V. Zhukov, I. Popova, and J. T. Yates, J. Vac. Sci. Technol. A **17**, 1727 (1999).

[45]T. Kubart, M. Aiempanakit, J. Andersson, T. Nyberg, S. Berg, and U. Helmersson, Surf. Coat. Technol. **205**(Suppl 2), S303 (2011).

[46]D. J. Christie, J. Vac. Sci. Technol. A **23**, 330 (2005).

[47]J. Vlcek and K. Burcalova, Plasma Sources Sci. Technol. **19**, 065010 (2010).

[48]T. Kozak and J. Vlcek, J. Phys. D: Appl. Phys. **49**, 055202 (2016).

[49]S. Kadlec and J. Capek, in *Reactive Sputter Deposition 2014* (Ghent, Belgium, 2014).

[50]M. A. Raadu, I. Axnas, J. T. Gudmundsson, C. Huo, and N. Brenning, Plasma Sources Sci. Technol. **20**, 065007 (2011).

[51]C. Huo, Ph.D. thesis, KTH Royal Institute of Technology, 2013.

[52]C. Q. Huo, D. Lundin, M. A. Raadu, A. Anders, J. T. Gudmundsson, and N. Brenning, Plasma Sources Sci. Technol. **22**, 045005 (2013).

[53]C. Q. Huo, M. A. Raadu, D. Lundin, J. T. Gudmundsson, A. Anders, and N. Brenning, Plasma Sources Sci. Technol. **21**, 045004 (2012).

[54]G. D. Stancu, N. Brenning, C. Vitelaru, D. Lundin, and T. Minea, Plasma Sources Sci. Technol. **24**, 045011 (2015).

[55]J. T. Gudmundsson and E. G. Thorsteinsson, Plasma Sources Sci. Technol. **16**, 399 (2007).

[56]M. Aiempanakit, A. Aijaz, D. Lundin, U. Helmersson, and T. Kubart, J. Appl. Phys. **113**, 133302 (2013).

[57]M. Palmucci, N. Britun, S. Konstantinidis, and R. Snyders, J. Appl. Phys. **114**, 113302 (2013).

[58]W. J. Moore and W. J. Moore, *Schrödinger: Life and Thought* (Cambridge University Press, 1992).

[59]K. Sarakinos, J. Alami, C. Klever, and M. Wuttig, Surf. Coat. Technol. **202**, 5033 (2008).

[60]T. I. Selinder, E. Coronel, E. Wallin, and U. Helmersson, Int. J. Refract. Met. Hard Mater. **27**, 507 (2009).

[61]M. Audronis and V. Bellido-Gonzalez, Thin Solid Films **518**, 1962 (2010).

[62]M. Audronis, V. Bellido-Gonzalez, and B. Daniel, Surf. Coat. Technol. **204**, 2159 (2010).

[63]M. Audronis and V. Bellido-Gonzalez, Surf. Coat. Technol. **205**(Suppl. 2), S322 (2011).

[64]M. Audronis and V. Bellido-Gonzalez, Surf. Coat. Technol. **205**, 3613 (2011).

[65]M. Aiempanakit, T. Kubart, P. Larsson, K. Sarakinos, J. Jensen, and U. Helmersson, Thin Solid Films **519**, 7779 (2011).

[66]M. Hala, J. Capek, O. Zabeida, J. E. Klemberg-Sapieha, and L. Martinu, J. Phys. D: Appl. Phys. **45**, 055204 (2012).

[67]C. Nouvellon, M. Michiels, J. P. Dauchot, C. Archambeau, F. Laffineur, E. Silberberg, S. Delvaux, R. Cloots, S. Konstantinidis, and R. Snyders, Surf. Coat. Technol. **206**, 3542 (2012).

[68]A. Surpi, T. Kubart, D. Giordani, M. Tosello, G. Mattei, M. Colasuonno, and A. Patelli, Surf. Coat. Technol. **235**, 714 (2013).

[69]M. Hala, R. Vernhes, O. Zabeida, J. E. Klemberg-Sapieha, and L. Martinu, J. Appl. Phys. **116**, 213302 (2014).

[70]J. Kohout, E. Bousser, T. Schmitt, R. Vernhes, O. Zabeida, J. Klemberg-Sapieha, and L. Martinu, Vacuum **124**, 96 (2016).

[71]T. Shimizu, M. Villamayor, D. Lundin, and U. Helmersson, J. Phys. D: Appl. Phys. **49**, 065202 (2016).

[72]Y. P. Purandare, A. P. Ehiasarian, and P. E. Hovsepian, J. Vac. Sci. Technol. A **34**, 041502 (2016).

[73]D. Lundin, M. Cada, and Z. Hubicka, J. Vac. Sci. Technol. A **34**, 041305 (2016).

[74]S. Loquai, B. Baloukas, O. Zabeida, J. E. Klemberg-Sapieha, and L. Martinu, Sol. Energy Mater. Sol. Cells **155**, 60 (2016).